文章编号:1000-0887(2016)12-1345-14

Investigations of Self-Propulsion in Waves of Fully Appended ONR Tumblehome Model*

WANG Jian-hua, WAN De-cheng

(*State Key Laboratory of Ocean Engineering*(*Shanghai Jiao Tong University*);
School of Naval Architecture, Ocean & Civil Engineering, Shanghai Jiao Tong University;
Collaborative Innovation Center for Advanced Ship and Deep-Sea Exploration,
Shanghai 200240, *P.R.China*)

Abstract: In the present work, the CFD-based method coupled with the dynamic overset grid technique is applied to investigate the hydrodynamic performance of the fully appended ONR tumblehome ship model under self-propulsion condition in head waves. All the computations are carried out by our in-house CFD solver naoe-FOAM-SJTU and the overset grid module is used to update the ship motions with rotating propellers while a self-developed 3D wave tank module is applied to generate desired wave environment. The ship model is advancing at its model point obtained with previous CFD results in calm water and the simulation is according to the benchmark case from the Tokyo 2015 CFD Workshop in ship hydrodynamics. The predicted results, i.e. ship motions and instantaneous advancing speeds are presented and compared with the available experimental data. Propulsion coefficients, K_T and K_Q, as well as detailed information of the flow field are also given to explain the hydrodynamic performance during the self-propulsion in waves. Good agreements are achieved which indicate that the present approach is applicable for the direct simulation of self-propulsion in waves.

Key words: self-propulsion in waves; dynamic overset grid; ship hydrodynamics; naoe-FOAM-SJTU solver

CLC number: U661.1; O242; O359 **Document code**: A

doi: 10.21656/1000-0887.370525

Introduction

Self-propulsion and seakeeping are two key standards to examine a ship's safety and powering performance. The wave loads, ship motions and propeller characteristics of a self-propelled ship in waves are of great complexity. For the fully appended ship, the flow field around the hull and appendages can be even more complicated. Generally, the sea states for the free running ships will always come with rough waves, which means that the seakeeping and propulsion will influence each other. However, most previous studies fo-

* Received 2016-11-17; Revised 2016-11-29
Project supported by the National Natural Science Foundation of China (51379125; 51490675; 11432009; 51579145; 11272120) and the Chang Jiang Scholars Program of China(T2014099)
Corresponding author, WAN De-cheng, E-mail: dcwan@sjtu.edu.cn

cused on either seakeeping of bare hull or self-propulsion in calm water. The direct study of self-propulsion in waves is rarely seen due to its complexity.

Seakeeping is a conventional problem for ship hydrodynamics and the studies in this area have been extensively advanced[1-3]. Potential flow methods are firstly used to predict seakeeping characteristics but have limitations when handling strong nonlinear problems. CFD methods, especially the Reynolds-averaged Navier-Stokes (RANS) approach coupled with the deforming mesh technology, consider viscous effects and can resolve nonlinear waves, but are still limited to relatively small ship motions[4]. These two traditional methods can only be applied to study the seakeeping performance of bare hull models due to their drawbacks mentioned above.

Self-propulsion simulation requires the capabilities of 6 degrees of freedom (6DOF) modules with a hierarchy of bodies in a free surface environment. To perform the CFD simulation of self-propulsion, a fully discretized module of the moving ship hull, the rotating propeller and the moving rudder is the one least reliant on geometries and is of high accuracy. The dynamic overset grid method, including a hierarchy of bodies that enable computation of full 6DOF and moving components (rudders, propellers), makes it possible to directly simulate self-propulsion. Recently, the overset grid method has been successfully applied to the computations of ship hydrodynamics, especially for the direct simulation of hull-propeller-rudder interaction in calm water. Carrica et al.[5] performed self-propulsion computations using a speed controller and a discretized propeller with dynamic overset grids, which shows that direct simulation of self-propelled ships is feasible. Broglia et al.[6-7] used the same approach to simulate the turning circle maneuver of a fully appended twin-screw vessel with a finite volume method CFD solver. Further analysis of the distributions of forces and moments on the hull, appendages and rudders has been done to obtain the hydrodynamic behavior in turning tests. Shen et al.[8] implemented the dynamic overset grid module to OpenFOAM and conduted the computation of KCS self-propulsion and zigzag maneuvering. The comparisons between computations and experiments are highly satisfactory, which confirms that the overset grid method is preferable for the direct simulation of ship-hull-rudder interaction.

Simulation of self-propulsion in waves requires the capabilities of handling large-amplitude ship motions in a violent free surface compared with the calm water conditions. In this paper, an incompressible RANS approach with the dynamic overset grid method is applied to simulate self-propulsion of fully appended ONR tumblehome ship models in head waves. And the outline of this paper goes as follows: first, a brief introduction is given; and section 1 presents the mathematical and numerical modeling, where the governing equations, the dynamic overset grid and the wave generation and absorption will be described in detail; section 2 relates the geometry and simulation design, including the geometry model, the grid distribution and the test conditions; then comes section 3 with the simulation results and analysis; finally, the conclusions of this study are summarized.

1 Mathematical and numerical modeling

1.1 Governing equations

The computations are performed with CFD solver naoe-FOAM-SJTU[9], which is developed on the open source platform OpenFOAM[10]. The present CFD code solves the RANS equations for unsteady turbulent flows around the complex geometry models. The turbulence is simulated with a blended $(k\text{-}\omega)/(k\text{-}\varepsilon)$ shear stress transport (SST) turbulence model[11] and the near-wall treatment is by means of the wall functions. The unsteady RANS equations are presented as a mass conservation equation and a momentum conservation equation:

$$\nabla \cdot \boldsymbol{U} = 0, \tag{1}$$

$$\frac{\partial \rho \boldsymbol{U}}{\partial t} + \nabla \cdot [(\rho \boldsymbol{U} - \boldsymbol{U}_g)\boldsymbol{U}] = -\nabla p_d - \boldsymbol{g} \cdot \boldsymbol{x} \nabla \rho + \nabla \cdot (\mu_{eff} \nabla \boldsymbol{U}) + (\nabla \boldsymbol{U}) \cdot \nabla \mu_{eff} + \boldsymbol{f}_s, \tag{2}$$

where $\boldsymbol{U}$ is the fluid velocity field and $\boldsymbol{U}_g$ is the grid velocity; $p_d = p - \rho \boldsymbol{g} \cdot \boldsymbol{x}$ is the dynamic pressure; ρ is the mixture density of the two-phase fluid; $\boldsymbol{g}$ is the gravitational acceleration; $\mu_{eff} = \rho(\nu + \nu_t)$ is the effective dynamic viscosity, where ν and ν_t are the kinematic viscosity and kinematic eddy viscosity respectively, the latter one can be obtained with the turbulence model; $\boldsymbol{f}_s$ is the source term for sponge layer, which will be described in subsection 1.3.

The methodology uses a VOF approach with the bounded compression technique to capture free surface and the transport equation is expressed as

$$\frac{\partial \alpha}{\partial t} + \nabla \cdot [(\boldsymbol{U} - \boldsymbol{U}_g)\alpha] + \nabla \cdot [\boldsymbol{U}_r(1 - \alpha)\alpha] = 0, \tag{3}$$

where α is the volume of fraction, 0 and 1 represent air and water respectively and $0 < \alpha < 1$ stands for the interface between two-phase fluid. $\boldsymbol{U}_r$ is the velocity field used to sharpen the interface while "$\nabla \cdot$" guarantees conservation and $(1 - \alpha)\alpha$ guarantees boundedness. Detailed information of the implementation of bounded compression techniques in OpenFOAM can be found in ref. [12].

The finite volume method (FVM) with unstructured grids is used to transform the equations from the physical space into the computational space. The solution of the governing equations is achieved by using the pressure implicit with splitting of operator (PISO) algorithm[13]. Furthermore, several built-in numerical schemes in OpenFOAM are used to solve the partial differential equations (PDE). The 2nd-order backward Euler scheme is used for temporal discretization. The 2nd-order TVD scheme is used to discretize the convection terms, while a central differencing scheme is applied for the viscous terms.

1.2 Dynamic overset grid

The dynamic overset grid is the key point for direct simulation of the complex motions with a hierarchy of bodies. Generally, an overset grid comprises two or more blocks of overlapping structured or unstructured grids, and the overlapping grids can move independently without constraints. In the dynamic overset computation process, the grids in the computational domain are first classified into several types according to their locations,

such as fringe cells, hole cells and donor cells etc. The fringe cell has a stencil consisting of several donor cells that provide information to it from the donor grid. The value of variable ϕ of the fringe cell is obtained through interpolation from the donor cells:

$$\phi = \sum_{i=1}^{n} \omega_i \cdot \phi_i , \tag{4}$$

$$\sum_{i=1}^{n} \omega_i = 1 , \tag{5}$$

where ω_i is the weight coefficient and ϕ_i is the donor cell value for each donor i. The weight coefficient is obtained by a clipped Laplace weight[14], which is proved to be stable and in 2nd-order accuracy. The information mentioned above is called the domain connectivity information (DCI). In the present work, Suggar++[15] is utilized to obtain the DCI at run time. To combine OpenFOAM with Suggar++, a communication, which is responsible for DCI exchange between the OpenFOAM processor and the Suggar++ processor, has been implemented using the message passing interface (MPI) library[8]. Other features consist of a full 6DOF motion module with a hierarchy moving components and several modifications for sparse matrix solvers and the MULES solver to exclude non-active cells.

The 6DOF motion solver with the dynamic overset grid capability allows the ship hull as well as the moving components to move simultaneously. Two coordinate systems are used to solve the 6DOF equations. One is the inertial system (earth-fixed system) and the other is the non-inertial system (ship-fixed system). The inertial system can be fixed to earth or move at a constant speed with respect to the ship but not allowed to pitch, heave or roll so that can keep the free surface horizontal. The non-inertial system is fixed to the ship and can translate or rotate according to its motions. Details of the 6DOF motion with a hierarchy of bodies and overset grid module implementation can be found in Shen et al.[8]. In our present study, the complex geometry is decomposed into several overlapping grids, and can be used to handle complex ship motions with moving components.

1.3 Wave generation and absorption

The wave generation and absorption are achieved with the self-developed numerical wave tank module in the naoe-FOAM-SJTU solver. Only a brief introduction is presented herein, and detailed information can be seen in Cao et al.[16-17] and Shen et al.[18]. The schematic of the wave generation and absorption is shown in fig. 1. A fixed inlet wave boundary condition is applied to generate desired waves. Boundary conditions of $\boldsymbol{U}(u,v,w)$ in RANS equations can be directly adopted as the Dirichlet condition with the specified wave theory. The 1st-order Stokes wave theory in deep water is adopted herein, and the expressions are as follow:

$$\begin{cases} \eta = a\cos(\boldsymbol{k}\cdot\boldsymbol{x} - \omega t + \delta), \\ u = a\omega e^{kz}\cos(\boldsymbol{k}\cdot\boldsymbol{x} - \omega t + \delta), \\ v = a\omega e^{kz}\cos\beta\cos(\boldsymbol{k}\cdot\boldsymbol{x} - \omega t + \delta), \\ w = a\omega e^{kz}\sin\beta\cos(\boldsymbol{k}\cdot\boldsymbol{x} - \omega t + \delta), \end{cases} \tag{6}$$

where η is the desired wave elevation and u, v, w are the wave velocity boundary conditions, $\boldsymbol{k}$ is the wave number presented as a vector that includes the wave direction, δ is the

wave phase, β is the wave direction defined as the angle between the ship advancing direction and the wave direction. For instance, $\beta = 0°$ is head wave and $\beta = 90°$ is beam wave.

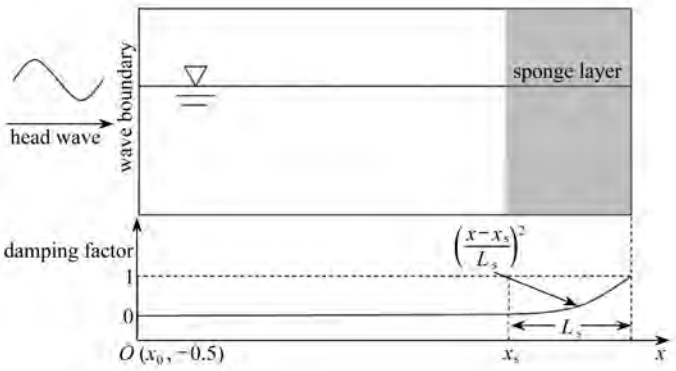

Fig. 1 Schematic of the wave generation and absorption

The boundary condition for α is more complicated compared with the velocity boundary. When the cell of the inlet boundary is totally below the transient wave elevation, the value of α is 1, otherwise α is 0. If the wave elevation is across the boundary cell, α can be obtained as

$$\alpha = \frac{S_w}{S_0}, \tag{7}$$

where S_0 is the total area of the cell face and S_w is the wetted face area.

The wave damping zone, also called the sponge layer, is set ahead the outlet boundary with a certain length.The wave can be absorbed by adding a source term in the momentum equation, which is written as

$$\boldsymbol{f}_s(x) = \begin{cases} -\rho\alpha_s\left(\dfrac{x - x_s}{L_s}\right)^2(\boldsymbol{U} - \boldsymbol{U}_{ref}), & x_s < x \leqslant L_s, \\ \boldsymbol{0}, & x_0 < x \leqslant x_s, \end{cases} \tag{8}$$

where x_0 is the offset of the inlet boundary and x_s is the start position of sponge layer, L_s is the length of layer, α_s is a dimensionless artificial viscosity parameter to control wave damping effect. The wave damping factor along the wave tank is also shown fig. 1. This method has been extensively validated in the previous work[16-18].

2 Geometry and simulation design

2.1 Geometry model

The self-propulsion simulation in waves is carried out for ONR tumblehome model 5613, which is a preliminary design of a modern surface combatant fully appended with skeg and bilge keels. In addition, the model is equipped with rudders, shafts and propellers with propeller shaft brackets. The geometry model of ONR tumblehome is shown in fig. 2, and the main geometric characteristics are listed in table 1. The ship model was used as one of the benchmark cases in the Tokyo 2015 CFD Workshop in ship hydrodynamics. Extensive experiments[19] were performed in IIHR for this ship model and the available experimental data can be used to validate our computational results.

Fig. 2 The geometry model of ONR tumblehome

Table 1 Main parameters of the ship model

parameter	model scale	full scale
length of waterline L_{WL} /m	3.147	154.0
width of waterline B_{WL} /m	0.384	18.78
draft T /m	0.112	5.494
displacement Δ /kg	72.6	8.507E6
propeller diameter D_P /m	0.106 6	
propeller shaft angle① ε /(°)	5	
propeller rotation direction D_r	inward	inward
maximum rudder rate r_m /((°)/s)	35.0	

Before the simulation, a simple hydrostatic computation is firstly performed to obtain the longitudinal location of the center of gravity, the mass and the static wetted area of the ship in static condition. The resulting mass of the ship model is 0.07% larger than the experiment. The small deviation is due to the fact that the geometry is discretized in space.

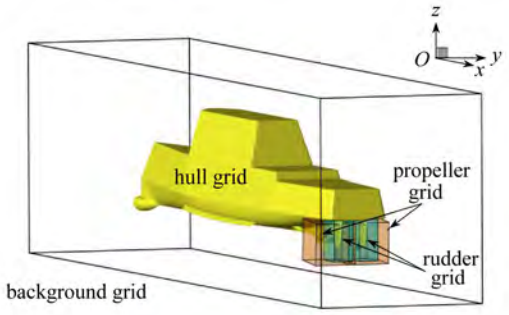

Fig. 3 The overset grid arrangement

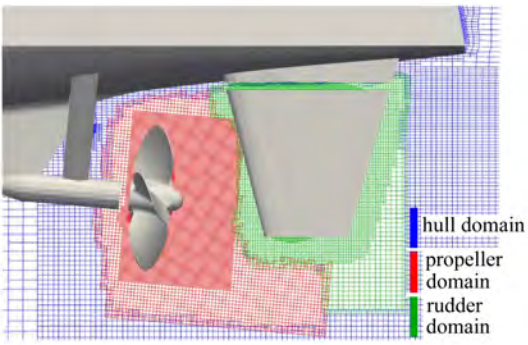

Fig. 4 The local grid distribution

2.2 Grid distribution

In the present study, the computational domain is divided into 6 parts: one for the background grid, one for the grid around the ship hull, two for the grids around propellers on the starboard side and the port side, two for both side rudders. The background domain extends to $-1.5L_{WL} < x < 3.0L_{WL}$, $-1.5L_{WL} < y < 1.5L_{WL}$, $-1.0L_{WL} < z < 0.5L_{WL}$, and the hull domain is much smaller with a range of $-0.15L_{WL} < x < 1.2L_{WL}$, $-0.13L_{WL} < y < 0.13L_{WL}$, $-0.2L_{WL} < z < 0.2L_{WL}$. Fully unstructured grids are generated by snappyHexMesh with the background grid generated by blockMesh, both of which are pre-processing utilities provid-

① Downward positive for the shaft angle and rotation direction views from the stern.

ed by OpenFOAM. The overset grid arrangement and the local mesh distribution is shown in fig. 3 and fig. 4 respectively. The total grid number for the self-propulsion simulation in waves is 6.83×10^6 and the detailed grid information in each part is shown in table 2. The motion level of the 6 parts of overlapping grids are also shown in the table, where the ship hull is solved as the parent level of the 6DOF motion and the background grid can move with it in horizontal motion, while the twin propeller grids and rudder grids are children to the ship, and move according to the control laws. During the computation, the propeller grids rotate as a rigid body with 1DOF, and the rotational angle is controlled by the speed controller.

Table 2 The grid information in each part

grid	total	port	starboard	level
background	1.36×10^6	–	–	root
hull	2.61×10^6	–	–	parent
propeller	2.28×10^6	1.14×10^6	1.14×10^6	children
rudder	0.58×10^6	0.29×10^6	0.29×10^6	children
total	6.83×10^6	–	–	–

As for the boundary conditions for the computational domain, the upstream inlet is of the wave generation boundary, where the velocity condition is according to the specified wave theory mentioned in the wave generation part; side boundaries are identical to zero velocity and zero gradient of pressure; moving bodies are non-slip on all solid surfaces, where $\boldsymbol{U}=\dot{\boldsymbol{x}}$, $\partial p/\partial n=0$, and the downstream outlet boundary ($\partial^2\boldsymbol{U}/\partial n^2=\boldsymbol{0}$, $\partial p/\partial n=0$).

Note that artificial gaps between propellers and shafts, rudders and rudder roots are applied to obtain enough overlapping grids for the overset grid interpolation. After all the grids are generated, a preprocessing step requires setting up the overset grid inputs and running Suggar++ with appropriate boundary conditions, with the purpose of testing that valid interpolations exists.

2.3 Test conditions

The present work is a benchmark case of the Tokyo 2015 CFD Workshop for ONR tumblehome model. According to the case setup, the fully appended ship is set to advance at the model point in head waves with rotating propellers. The target ship speed is $U=1.11$ m/s ($Fr=0.20$) with wave conditions of $\lambda/L_{WL}=1.0$, $H/\lambda=0.02$, where λ is the wave length and H is the wave height.

The computations were carried out in a HPC cluster (IBM nx360M4), which consisted of 20 CPUs per node and a 64 GB accessible memory. 40 processors were assigned to calculate the self-propulsion computation in waves, in which 38 processors are for the flow calculation and the other 2 processors for the DCI computation with Suggar++. The time step was set to $\Delta t=0.000\,5$, corresponding to approximately 1.5degs of propeller rotation per time step in the self-propulsion condition. The time to complete the computation was approximately 225 wall clock hours with about 38 000 time steps.

3 Numerical results and analysis

In order to conduct the simulations of self-propulsion in waves, the model point for

the self-propelled ship model has to be calculated first, which means that the simulation of self-propulsion in calm water should be conducted to obtain the model point at the desired ship speed. In the calm water case, a feedback PI controller is used to achieve the self-propulsion point. This work was done earlier, which also included grid convergence studies and validations against available experimental results, and the detailed information can be found in Wang et al.[20]. The propeller rotational speed is well predicted with a difference of 1.7% with respect to the experimental data. The good agreement indicates that the present approach is suitable for the self-propulsion simulation.

Simulations of the self-propelled ONR tumblehome ship model in head waves are performed at a wave length of 3.147 m and a wave height of 0.062 94 m. The rotational speed of propellers is set to the previous predicted value of 8.81 r/s. In this paper all variables are non-dimensionalized with reference velocity U_0 in model scale, ship water length L_{WL}, wave amplitude ζ_a and wave number k. The resulting conditions are Reynolds number $Re = (U_0 L_{WL})/\nu = 3.39 \times 10^6$ and Froude number $Fr = U_0/\sqrt{gL_{WL}} = 0.2$.

3.1 Motions and propulsive coefficients

Mimicking the experiment data, the simulation first starts from the final state of self-propulsion in calm water and the ship is released when the wave crest is located at the bow. Fig. 5 shows the simulation results of the time histories of ship motions. The predicted heave and pitch motions show satisfactory agreement with the experimental results for both amplitudes and frequencies. The overall agreement shows that the present approach can simulate the motion response with high accuracy. 4 typical moments in 1 wave period, A, B, C, D corresponding to the moments shown in fig. 5(a), are chosen to further analyze the hydrodynamic performance in the self-propulsion condition in waves. As for ship speed u, the curves show significant speed loss due to the added resistance induced by the incident waves both in numerical and experimental results. The present results match well with the overall trend of the measurement, but experience a larger speed loss. This is mainly due to the fact that the RANS approach may result in larger viscous effect, and lead to larger predicted resistance.

To further analyze the propulsive performance, the non-dimensional coefficients are used and the expressions are as follow:

$$K_T = \frac{T}{\rho n^2 D_P^4}, \tag{9}$$

$$K_Q = \frac{Q}{\rho n^2 D_P^5}, \tag{10}$$

where T and Q are the thrust and torque respectively, n is the propeller rotational speed and D_P the propeller diameter. Fig. 6 shows the propulsive coefficients, i.e. K_T and $10K_Q$, during the simulation time. Both the thrust and torque coefficients are evidently related to the ship motions. The thrust coefficient is the maximum when the ship bow goes up and reaches minimum when the bow goes down. The same trend occurs with the torque coefficients. The variation of propulsion coefficients shows strong accordance with the speed loss presented in fig. 5(c). For instance, at time B, the actual ship speed is larger and results in lar-

ger inflow of the propeller, which further leads to the increase of thrust. Better understanding of this phenomenon will be shown in the following flow visualization part. Besides, high frequency fluctuations in the thrust and torque coefficients that correlate with the blade passage frequency are presented, which can be obviously seen in the partial enlarged view.

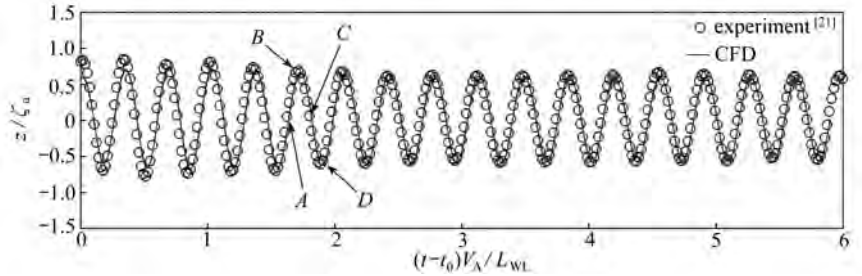

(a) The heave motion

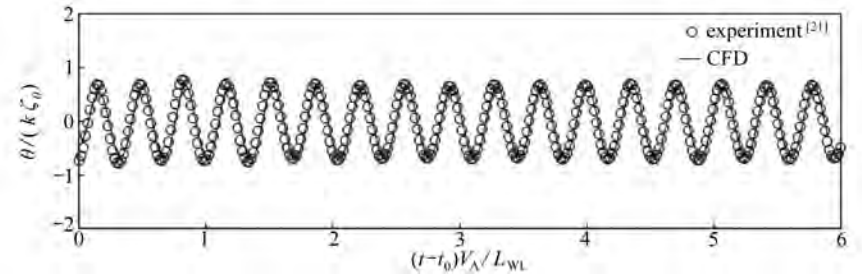

(b) The pitch motion

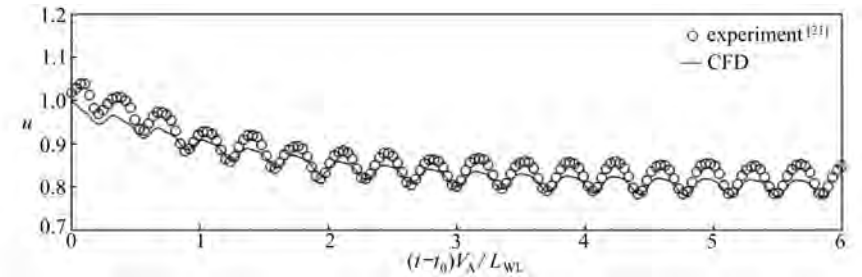

(c) The ship speed

Fig. 5 The heave, pitch and ship speed results

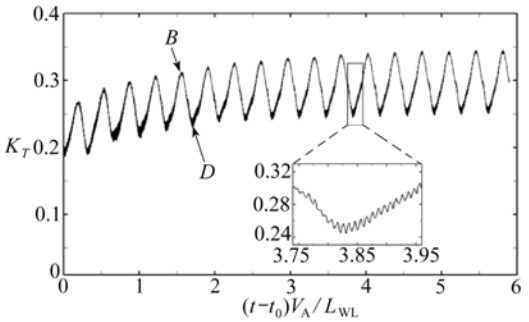

(a) K_T

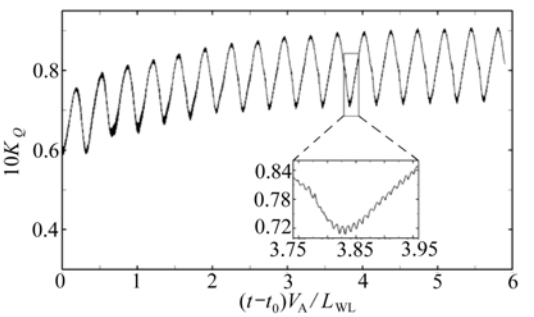

(b) $10K_Q$

Fig. 6 Time histories of propulsive coefficients

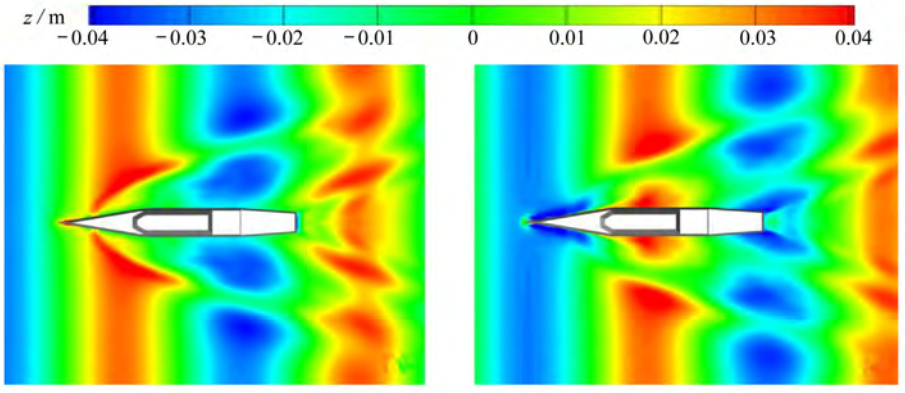

(a) Time A: $t = T_0$ (b) Time B: $t = T_0 + 0.25T$

(c) Time C: $t = T_0 + 0.5T$ (d) Time D: $t = T_0 + 0.75T$

Fig. 7 The free surfaces colored with wave elevations

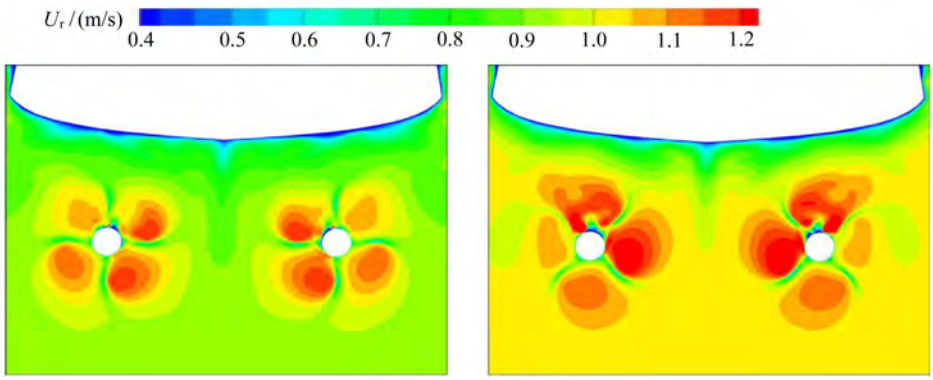

(a) Time B: $t = T_0 + 0.25T$ (b) Time D: $t = T_0 + 0.75T$

Fig. 8 Wake profiles ahead of the twin propellers colored with relative axial velocity $U_r = U_0 - U_x$

3.2 Flow visualizations

Though experiments are still playing an important role in the free running tests, the CFD is becoming undeniably attractive for the numerical analysis and visualizations of the flow field. Fig. 7 shows 4 instantaneous snapshots of free surface in one wave period. From the figure one can see that the wave diffraction is considerable at relatively low speed $Fr = 0.2$.

An interesting phenomenon was observed that when the forehead of the ship bows down (time D: $t = T_0 + 0.75T$), a new wave crest occurs after the incident wave crest.

To further explain the propulsion performance with thrust and torque, the wake profile ahead of the twin propellers is presented (fig. 8). 2 snapshots corresponding to times B and D are shown. The flow field is colored with relative axial velocity $U_r = U_0 - U_x$ for better visualization. The relative inflow at time B is obviously smaller than that at time D, which means that the actual inflow is in the opposite way. This enables a better understanding of the variation of propulsive coefficients explained in the part before.

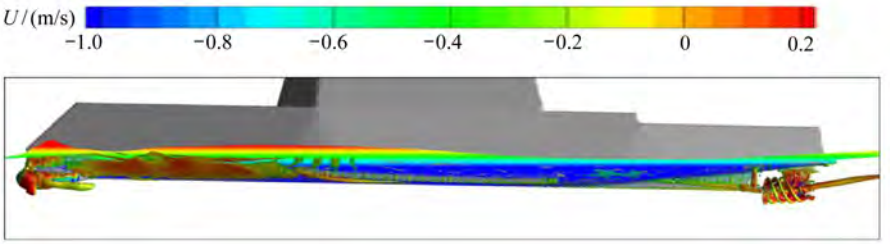

(a) Time A: $t = T_0$

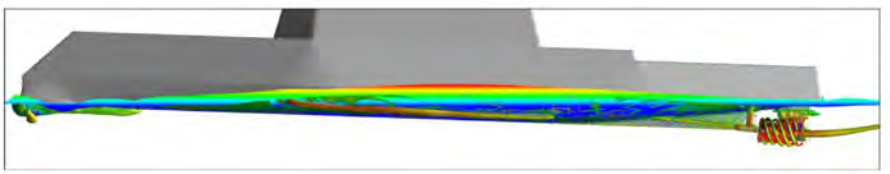

(b) Time B: $t = T_0 + 0.25T$

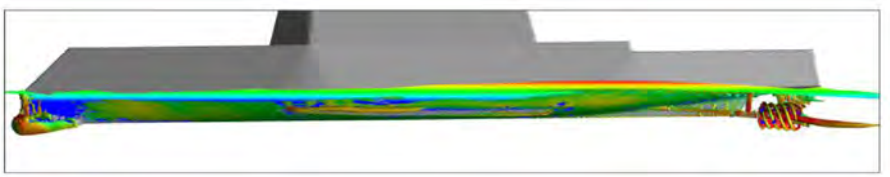

(c) Time C: $t = T_0 + 0.5T$

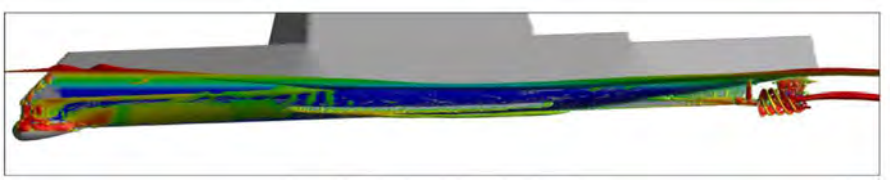

(d) Time D: $t = T_0 + 0.75T$

Fig. 9 The vortical structures depicted as iso-surfaces for $Q = 200$ colored with axial velocity U

Fig. 9 shows profile views of the ship in the 4 quarter periods in head waves with vortical structures depicted as iso-surfaces for $Q = 200$ colored with the axial velocity. The 2 peak phenomena in free surface mentioned above can be clearly seen in fig. 9(d). Corresponding to the wave elevation shown in fig. 7, the ship bow goes up when experiencing the wave trough, and falls down with the wave crest. The ship bow is exposed at time B and the tran-

som stern is dry at time C, which will strongly influence the strengths of the vorticities and propulsive coefficients. The propeller produces strong tip and hub vortices, which can be transported downstream as far as the grid is refined. The hub vortex of the propeller follows the trajectory of the ship motion in vertical direction with a certain delay in time. The bow vortex and bilge vortex can also be observed in the visualization and vary with the ship motions. Furthermore, strong interaction between the ship hull, propellers and rudders can be easily seen. The tip vortex of the propeller is strongly influenced by the following rudder. In addition, the rudder root vortex also appears after the artificial gap between the moving rudder and the rudder root, which is not a real physical flow phenomenon.

4 Conclusions

In this paper, direct computations of self-propulsion in waves for fully appended ONR tumblehome models are conducted. The self-propelled ship is set to advance at the model point (8.81 r/s) and the target ship speed is U_0 = 1.11 m/s with wave conditions of λ/L_{WL} = 1.0, H/λ = 0.02. Predicted ship motions including heave, pitch and advancing speed are presented and compared with the experimental data. The motion responses in head waves show satisfactory agreement with the measurements both in amplitudes and frequencies. A significant speed loss is also observed in the predicted results and matches well with the experimental data. Propulsive coefficients K_T and $10K_Q$, are also presented to show the propulsion performance during self-propulsion in waves. Furthermore, high frequency fluctuations in thrust and torque coefficients that correlate with the blade passage frequency are observed in the CFD results. While the simulation results and comparisons with the measurement data show that the present CFD method coupled with the dynamic overset grid approach is suitable for the direct computations of self-propulsion in waves, the computational cost is still very high, taking about 2 weeks to perform the simulations. The flow visualizations, i.e. the free surface wave elevations in the inflow region ahead of twin propellers and the vortical structures, are also presented to better understand the variation of hydrodynamic performance within the self-propulsion in waves.

The future work includes the study of the course keeping for the free running ship model with more complex wave conditions, such as the beam waves and following waves. More emphases will be put on the investigation of the yaw motion with rudder control.

Acknowledgments

This work is supported by the National Natural Science Foundation of China (51379125; 51490675; 11432009; 51579145; 11272120); the Chang Jiang Scholars Program of China (T2014099); the Program for Professor of Special Appointment (Eastern Scholar) at Shanghai Institutions of Higher Learning (2013022) and the Innovative Special Project of Numerical Tank of Ministry of Industry and Information Technology of China (2016-23/09), to which the authors are most grateful.

References:

[1] Simmonsen C D, Otzen J F, Joncquez S, Stern F. EFD and CFD for KCS heaving and pitching

in regular head waves[J]. *Journal of Marine Science and Technology*, 2013, **18**(4): 435-459.

[2] SHEN Zhi-rong, YE Hai-xuan, WAN De-cheng. Motion response and added resistance of ship in head waves based on RANS simulations[J]. *Chinese Journal of Hydrodynamics*, 2012, **27**(6): 621-633.

[3] Sato Y, Miyata H, Sato T. CFD simulation of 3-dimensional motion of a ship in waves: application to an advancing ship in regular heading waves[J]. *Journal of Marine Science and Technology*, 1999, **4**(3): 108-116.

[4] SHEN Zhi-rong, WAN De-cheng. RANS computations of added resistance and motions of a ship in head waves[J]. *International Journal of Offshore and Polar Engineering*, 2013, **23**(4): 264-271.

[5] Carrica P M, Wilson R V, Noack R W, Stern F. Ship motions using single-phase level set with dynamic overset grids[J]. *Computers & Fluids*, 2007, **36**(9): 1415-1433.

[6] Broglia R, Dubbioso G, Durante D, di Mascio A. Turning ability analysis of a fully appended twin screw vessel by CFD. Part I: single rudder configuration[J]. *Ocean Engineering*, 2015, **105**: 275-286.

[7] Dubbioso G, Durante D, di Mascio A, Broglia R. Turning ability analysis of a fully appended twin screw vessel by CFD. Part II: single vs twin rudder configuration[J]. *Ocean Engineering*, 2016, **117**: 259-271.

[8] SHEN Zhi-rong, WAN De-cheng, Carrica P M. Dynamic overset grids in OpenFOAM with application to KCS self-propulsion and maneuvering[J]. *Ocean Engineering*, 2015, **108**: 287-306.

[9] Shen Z, Cao H, Ye H, Wan D. The manual of CFD solver for ship and ocean engineering flows: naoe-FOAM-SJTU[R]. Shanghai Jiao Tong University, 2012.

[10] Jasak H, Jemcov A, Tukovi$\acute{c}$ Z. OpenFOAM: a C++ library for complex physics simulations [C]//*Proceedings of International Workshop on Coupled Methods in Numerical Dynamics*. Dubrovnik, Croatia: IUC, 2007.

[11] Menter F R. Review of the shear-stress transport turbulence model experience from an industrial perspective[J]. *International Journal of Computational Fluid Dynamics*, 2009, **23**(4): 305-316.

[12] Weller H G. A new approach to VOF-based interface capturing methods for incompressible and compressible flow[R]. Report TR/HGW/04, OpenCFD Ltd, 2008.

[13] Issa R I. Solution of the implicitly discretised fluid flow equations by operator-splitting[J]. *Journal of Computational Physics*, 1986, **62**(1): 40-65.

[14] Holmes D G, Connell S D. Solution of the 2D Navier-Stokes equations on unstructured adaptive grids[C]//*9th Computational Fluid Dynamics Conference*. Buffalo, New York, USA: AIAA-89-1932, 1989.

[15] Noack R W, Boger D A, Kunz R F, Carrica P M. Suggar++: an improved general overset grid assembly capability[C]//*19th AIAA Computational Fluid Dynamics, Fluid Dynamics and Co-located Conferences*. San Antonio, Texas, 2009.

[16] CAO Hong-jian, WAN De-cheng. Development of multidirectional nonlinear numerical wave tank by naoe-FOAM-SJTU solver[J]. *International Journal of Ocean System Engineering*, 2014, **4**(1): 52-59.

[17] CAO Hong-jian, WAN De-cheng. RANS-VOF solver for solitary wave run-up on a circular cylinder[J]. *China Ocean Engineering*, 2015, **29**(2): 183-196.

[18] SHEN Zhi-rong, WAN De-cheng. An irregular wave generating approach based on naoe-FOAM-

SJTU solver[J]. *China Ocean Engineering*, 2016, **30**(2): 177-192.

[19] Sanada Y, Tanimoto K, Takagi K, Gui L, Toda Y, Stern F. Trajectories for ONR tumblehome maneuvering in calm water and waves[J]. *Ocean Engineering*, 2013, **72**: 45-65.

[20] Wang J, Zhao W, Wan D. Free maneuvering simulation of ONR tumblehome using overset grid method in naoe-FOAM-SJTU[C]//*31st Symposium on Naval Hydrodynamics*. Monterey, CA, USA, 2016.

[21] National Maritime Research Institute (NMRI). Tokyo 2015: a workshop on CFD in ship hydrodynamics[Z/OL]. (2015-12-02)[2016-12-08]. http:// www.t2015.nmri.go.jp.

全附体 ONRT 船模在波浪中自航的数值模拟

王建华, 万德成

(上海交通大学 船舶海洋与建筑工程学院; 海洋工程国家重点实验室(上海交通大学); 高新船舶与深海开发装备协同创新中心, 上海 200240)

摘要: 采用基于重叠网格技术的 CFD 方法数值研究了全附体 ONRT 船模在迎浪工况中自航的水动力特性.文中数值计算采用自主开发的面向船舶与海洋工程的 CFD 求解器 naoe-FOAM-SJTU.自航计算中船体运动及螺旋桨转动等通过重叠网格技术完成,波浪环境则采用求解器中的三维数值造波和消波模块实现.计算中自航船模的螺旋桨转速通过静水自航数值计算得出,波浪工况计算采用东京 2015 CFD 会议中标准算例进行设置.数值计算结果,如船体运动、实时航速变化等,与试验数据进行了对比分析.此外,给出了数值预报的推力和扭矩系数,并且通过详细的流场信息来分析和解释了船模在波浪中自航过程中的水动力变化情况.数值预报结果同试验值吻合较好,说明采用当前结合重叠网格技术和 CFD 的数值方法可以很好地预报波浪中自航问题.

关 键 词: 波浪中自航; 重叠网格; 船舶水动力学; naoe-FOAM-SJTU 求解器

基金项目: 国家自然科学基金(51379125; 51490675; 11432009; 51579145; 11272120); 长江学者奖励计划(T2014099)

引用本文/Cite this paper:

WANG Jian-hua, WAN De-cheng. Investigations of self-propulsion in waves of fully appended ONR tumblehome model[J]. *Applied Mathematics and Mechanics*, 2016, **37**(12): 1345-1358.

王建华, 万德成. 全附体 ONRT 船模在波浪中自航的数值模拟[J]. 应用数学和力学, 2016, **37**(12): 1345-1358.